Radiation Physics and Chemistry 124 (2016) 91–98

Contents lists available at ScienceDirect

Radiation Physics and Chemistry

journal homepage: www.elsevier.com/locate/radphyschem

Radiation-induced reduction of quinoxalin-2-one derivatives in aqueous solutions

Konrad Skotnicki [a], Julio R. De la Fuente [b], Alvaro Cañete [c], Krzysztof Bobrowski [a,*]

[a] Centre of Radiation Chemistry and Technology, Institute of Nuclear Chemistry and Technology, Dorodna 16, 03-195 Warsaw, Poland
[b] Departamento de Química Orgánica y Fisicoquímica, Facultad de Ciencias Químicas y Farmacéuticas, Universidad de Chile, Casilla 223, Santiago 1, Chile
[c] Departamento de Química Orgánica, Facultad de Química, Pontificia Universidad Católica de Chile, Casilla 306, Correo 22, Santiago, Chile

HIGHLIGHTS

- Rate constants $k(e^-_{aq} + Q/3-MeQ)$ have been determined at 25 °C at two pHs (7 and 13).
- Equilibrium constants ($pK_a \geq 13.5$) for the protropic equilibria have been provided.
- Spectral characteristics for $Q^{\bullet -}$/3-$MeQ^{\bullet -}$ and $QH^{\bullet}$/3-$MeQH^{\bullet}$ have been determined.
- The most stable hydrogenated radicals ($QH^{\bullet}$ and 3-$MeQH^{\bullet}$) have been defined.

ARTICLE INFO

Article history:
Received 22 October 2015
Received in revised form
2 December 2015
Accepted 11 December 2015
Available online 15 December 2015

Keywords:
Quinoxalin-2-ones
Pulse radiolysis
Hydrated electrons
Radical anions
Hydrogenated radicals
Prototropic equilibria

ABSTRACT

Quinoxaline-2-one derivatives have been proposed as potential drugs in treatments of various diseases since some of them showed a variety of pharmacological properties. The kinetics and spectral characteristics of the transients formed in the reactions of hydrated electrons (e^-_{aq}) with quinoxalin-2-(*1H*)-one (Q) and its methyl derivative, 3-methyl quinoxalin-2-(*1H*)-one (3-MeQ) were studied by pulse radiolysis in aqueous solutions at pH ranging from 5 to 14. The transient absorption spectra recorded in the reactions of (e^-_{aq}) with Q and 3-MeQ at pH 7 consisted of a broad, almost flat band in the range 390–450 nm and were assigned to the respective protonated radical anions ($QH^{\bullet}$/3-$MeQH^{\bullet}$) at N4 atom in a pyrazin-2-one ring. On the other hand, the transient absorption spectra recorded in the reactions of (e^-_{aq}) with Q and 3-MeQ at pH 13 are characterized by a broad band with a much better pronounced maximum at $\lambda_{max}=390$ nm and higher intensity (in comparison to that at pH 7) and were assigned to the respective radical anions ($Q^{\bullet -}$/3-$MeQ^{\bullet -}$). Both forms are involved in the prototropic equilibrium with the pK_a located at pH ≥ 13.5. The rate constants of the reactions of (e^-_{aq}) with Q and 3-MeQ were found to be at pH 7 $(2.6 \pm 0.1) \times 10^{10}\ M^{-1}\ s^{-1}$ and $(2.1 \pm 0.1) \times 10^{10}\ M^{-1}\ s^{-1}$ and at pH 13 $(1.6 \pm 0.1) \times 10^{10}\ M^{-1}\ s^{-1}$ and $(1.3 \pm 0.1) \times 10^{10}\ M^{-1}\ s^{-1}$, respectively. Semi-empirical quantum mechanical calculations reproduce fairly well the spectral features of the experimental absorption spectra and show that protonated radical anions at nitrogen atom (N4) in both molecules are the most stable hydrogenated radicals.

1. Introduction

Quinoxaline-2-one derivatives are particularly interesting since some of them showed a variety of pharmacological properties, such as antimicrobial (Ajani et al., 2010; El-Sabbagh et al., 2009; Sanna et al., 1998, 1999), antiviral (Xu et al., 2009), antifungal (Carta et al., 2002; Ingale et al., 2007; Sanna et al., 1999), anxiolytic (Ulrich et al., 1998), analgesic (Ingale et al., 2007), antiinflammatory (El-Sabbagh et al., 2009), antithrombotic (Ries et al., 2003; Willardsen et al., 2004), and antitumor (Hirai et al., 2011; Koth et al., 2007; Lawrence et al., 2001; Meyer et al., 2006) activities. Based on the computer modeling and "in vitro" studies, quinoxalin-2-ones have been proposed as potential drugs in treatments of various diseases (Carta et al., 2006). The Structure Activity Relationship (SAR) studies have revealed that quinoxalin-2-ones derivatives bound to proteins receptors (e.g. in Cdk) are generally located close to the adenosine triphosphate (ATP) binding pocket (Hirai et al., 2011; Mori et al., 2008). The fact that these compounds are bound in very specific position in proteins may have serious consequences in their interactions with either amino acid residues or radicals derived from them. Certain amino acids residues – tyrosine (Tyr), tryptophan (Trp),

* Corresponding author.
E-mail addresses: k.skotnicki@ichtj.waw.pl (K. Skotnicki), jrfuente@ciq.uchile.cl (J.R. De la Fuente), acanetem@uc.cl (A. Cañete), k.bobrowski@ichtj.waw.pl (K. Bobrowski).

http://dx.doi.org/10.1016/j.radphyschem.2015.12.008
0969-806X/

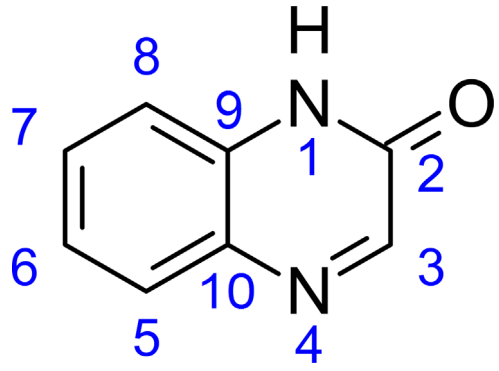

Chart 1. General structure of quinoxalin-2-ones.

and cysteine (Cys) are particularly vulnerable to oxidation. Therefore, the radical cations derived from quinoxalin-2-ones can modify these amino acids that are reasonably good electron donors and can be oxidized to tyrosyl (TyrO$^{\bullet}$), tryptophyl (TrpN$^{\bullet}$), and thiyl (CysS$^{\bullet}$) radicals, respectively. On the other hand, these radicals are reasonably good electron acceptors and can potentially act as oxidants of quinoxalin-2-ones intercalated in a protein matrix.

A key factor that is decisive in their biological activity is substitution at the carbon-3 in the pyrazine ring and at the carbons 6 and 7 in the benzene ring of the primary quinoxalin-2-one structure (Chart 1). Nearly all biologically active derivatives are substituted in those specific positions.

In order to address mentioned above oxidation processes involving quinoxalin-2-one derivatives, the kinetics and spectral characteristics of the transients formed in the reactions of $^{\bullet}$OH and $^{\bullet}N_3$ radicals with quinoxalin-2(1H)-one (Q) and 3-methyl-quinoxalin-2(1H)-one (3-MeQ) were studied by pulse radiolysis in aqueous solutions at pH 7. A primary distribution of the $^{\bullet}$OH attack was found nearly equal between benzene and pyrazin-2-one rings. Moreover, oxidation of Q and 3-MeQ by $^{\bullet}N_3$ with the rate constants similar to those measured for $^{\bullet}$OH suggests their rather low oxidation potential (Skotnicki et al., 2014).

Surprisingly, there are only a few reports about radical reduction processes involving quinoxalin-2-one derivatives. Some derivatives were found to initiate free radical polymerization by electron transfer from N-phenylglycine (Kucybala and Paczkowski, 1999; Kucybala et al., 2000). Their photoreduction by amines leads to the corresponding stable products dihydroquinoxalin-2-ones or the reductive dimers depending on the substituent in position 3 of the pyrazine ring (Nishio, 1990).

The photophysical and photochemical behavior of 1-methyl-3-phenyl-quinoxalin-2-one and 3-phenyl-quinoxalin-2-one in the presence of amines has been reported in some selected organic solvents (acetonitrile, methanol and hexane) (De la Fuente et al., 2002, 2000). Spectral and kinetic characteristics of the intermediate species: triplet ion-radical pairs ($Q^{\bullet -}$/amine$^{\bullet +}$) and hydrogenated neutral radicals (QH$^{\bullet}$) have been obtained by laser flash photolysis (De la Fuente et al., 2002). Calculated spectra using quantum mechanical semi-empirical AM1, PM3, and ZINDO/S approach were found to be in agreement with the experimental spectra (De la Fuente et al., 2002). Recently, the stable products resulting from the photoreduction of six 7-substituted-3-methyl-quinoxalin-2(*1H*)-one derivatives (substituents: H_3CO–, H_3C–, F–, H–, CF_3–, CN–) by α-amino-type radicals derived from N-phenylglycine (PhNHC$H_2^{\bullet}$) in acetonitrile solutions have been identified. Moreover, spectral and kinetic characteristics of the intermediate species: triplets (^{3}Q), radical anions ($Q^{\bullet -}$) and hydrogenated neutral radicals (QH$^{\bullet}$) have been obtained by laser flash photolysis in the presence of DABCO and N-phenylglycine (NPG) (De la Fuente et al., 2013).

The electrochemical studies of three 3-methyl-quinoxalin-2(1H)-ones: 3-methyl-quinoxalin-2(1H)-one, 3,6,7-trimethylquinoxalin-2(1H)-one and 7-amino-3-methyl-quinoxalin-2(1H)-one showed that the pyrazine ring is the electroactive center undergoing two-electron reduction (Zimpl et al., 2012).

Examples given above strongly indicate a necessity to gain a comprehensive and systematic knowledge about spectral and kinetic properties of radicals and radical ions derived from quinoxalin-2-ones. In particular, there is no information about the radicals and radical anions forming during reduction of these compounds. Therefore, in the current work we have investigated reduction processes in quinoxalin-2(1H)-one (Q) and its methyl derivative, 3-methyl-quinoxalin-2(1H)-one (3-MeQ) in aqueous solutions at pH ranging from pH 4 to 14, and starting from the primary transients formed by radiation-induced reduction by hydrated electrons (e^-_{aq}). These studies comprise spectral and kinetic properties of transients formed, including an assessment of the e^-_{aq} reactivity by determination of the respective second-order rate constants with quinoxalin-2-ones.

2. Materials and methods

2.1. Materials

Quinoxalin-2(1H)-one (2-quinoxalinol) (Q) was purchased from Aldrich and used without further purification. Nitrous oxide (N_2O) >98% was from Messer, Poland. 3-Methyl-quinoxalin-2(1H)-one (3-methyl-2-quinoxalinol) (3-MeQ) was prepared by the classical reaction of the corresponding o-phenyldiamine (1 mmol) by adding drop by drop methyl pyruvate (1.2 mmol) and triethylamine (3 mmol) in ethanol. A detailed description of the synthesis, purification and spectral characterization has been given elsewhere (De la Fuente et al., 2013).

All solutions were made with triply distilled water provided by a Millipore Direct-Q 3-UV system. The pH was adjusted by the addition of either $HClO_4$ or NaOH. Prior to irradiation, *tert*-butanol (0.5 M) was added to the samples which were subsequently purged gently with Ar for 30 min per 50 mL volume before experiments. The typical concentration of solutions in pulse radiolysis experiments was 0.1 mM of quinoxalin-2-ones unless otherwise specified.

2.2. UV–vis spectrophotometry

The absorption spectra were recorded with the JASCO V-670 UV–vis spectrophotometer using a 1 cm optical path length cell. Water without additives was used as a reference sample. An aliquot of 1 ml was taken to measure the absorption spectrum.

2.3. Pulse radiolysis

Pulse radiolysis experiments were performed with the INCT LAE 10 MeV linear accelerator with a typical pulse length of 8 ns. A detailed description of the experimental setup has been given elsewhere along with the basic details of the equipment and the data collection system (Bobrowski, 2005). Absorbed doses per pulse were on the order of 20 Gy (1 Gy=1 J kg^{-1}). Dosimetry was based on N_2O-saturated solutions containing 10^{-2} M KSCN, taking a radiation chemical yield of G=0.635 μmol J^{-1} and a molar absorption coefficient of 7580 M^{-1} cm^{-1} at 472 nm for the $(SCN)_2^{\bullet -}$ radical (Schuler et al., 1980). Experiments were performed with a continuous flow of sample solutions at room temperature (~23 °C).

2.4. Spectral analysis of time-resolved spectra

In any time window, following the electron pulse, the absorbance of the solution is related to the radiation chemical yield (G) and the molar absorption coefficients (ε) by the formula (1):

$$G \times \epsilon(\lambda j) = \Delta A(\lambda j)\frac{\epsilon_{472} G(SCN)_2^{\bullet -}}{\Delta A_{472}} \quad (1)$$

which are how to spectra are displayed in Figs. 1, 2, 4 and 5.

Eq. (1) is convenient way to normalize the absorbance $\Delta A(\lambda_j)$ to the radiation dose, the inverse of which is proportional to $\epsilon_{472} G$ ($(SCN)_2^{\bullet -}$)/ΔA_{472} from thiocyanate dosimetry, where ϵ_{472} is the molar absorption coefficient of $(SCN)_2^{\bullet -}$ at 472 nm, $G((SCN)_2^{\bullet -})$ is the radiation chemical yield of the $(SCN)_2^{\bullet -}$ radicals, and ΔA_{472} represents the observed absorbance change at $\lambda = 472$ nm in the thiocyanate dosimeter. The $G\epsilon(\lambda_j)$ are in turn related to the underlying transients via Beer's Law since $\Delta A = \log(I_0/I)$ is the absorbance of the sample.

2.5. Water radiolysis

During water radiolysis, e_{aq}^-, $^{\bullet}OH$, and $^{\bullet}H$ were generated with radiation chemical yields of 0.28, 0.28, and 0.06 μmol J^{-1}, respectively (Buxton et al. 2008). The reactions of hydrated electrons were studied in Ar-saturated solutions containing *tert*-butanol (0.5 M) in order to eliminate the contribution by the $^{\bullet}OH$ radicals. $^{\bullet}OH$ radicals are scavenged efficiently by reaction (2) with $k_1 = 6.0 \times 10^8$ M^{-1} s^{-1}, whereas $^{\bullet}H$ atoms react very slowly (reaction 3) with $k_2 = 1.7 \times 10^5$ M^{-1} s^{-1}

$$^{\bullet}OH + (CH_3)_3C\text{-}OH \rightarrow H_2C^{\bullet}(CH_3)_2C\text{-}OH + H_2O \quad (2)$$

$$^{\bullet}H + (CH_3)_3C\text{-}OH \rightarrow H_2C^{\bullet}(CH_3)_2C\text{-}OH + H_2 \quad (3)$$

The radiation chemical yield of $^{\bullet}H$ atoms at pH 7 was roughly 5-fold lower than that of $^{\bullet}e_{aq}^-$, the contribution of transient absorption spectra of products from $^{\bullet}H$ reactions with substrates was neglected.

In basic solutions (at pH > 13), the unscavenged $^{\bullet}H$ atoms are converted into e_{aq}^- according to reaction 4 with $k_3 = 2.2 \times 10^7$ M^{-1} s^{-1}: (Buxton et al., 1988a)

$$H^{\bullet} + OH^- \rightarrow e_{aq}^- \quad (4)$$

2.6. Calculations

Semi-empirical quantum mechanical calculations were made using HyperChem-8.0.3 by HyperCube, Inc.. The optimized structure geometries and the respective formation enthalpies were obtained by using the PM3 semi-empirical method with the UHF approximation and the proper charge and multiplicity: −-1 and 2 for the radical anions ($Q^{\bullet -}$/3-$MeQ^{\bullet -}$), and 0 and 2 for the protonated radical anions ($QH^{\bullet}$/3-$MeQH^{\bullet}$). The structures of these latter species were constructed by adding the H atom in the proper position of the ground state molecule whose geometry were first optimized by the Molecular Mechanic method MM^+ followed by the PM3/UHF calculation. The respective spectra were calculated by using ZINDO/S method applying the RHF approximation, even for radical species, and considering 10 occupied and 10 unoccupied molecular orbital. All the calculated spectra showed a large number of absorption lines in the high energy region of spectra below 300 nm that were not considered in this study because they are beyond the range of measurements, however, without affecting the spectral interest region. All the calculations were performed disregarding any solvent effect that likely will shift the calculated absorption by a few nm.

3. Results

3.1. Reactions of hydrated electrons with quinoxalin-2(1H)-one (Q) and 3-methyl-quinoxalin-2(1H)-one (3-MeQ)

The reactions of hydrated electrons (e_{aq}^-) with quinoxalin-2(1H)-one (Q) and 3-methyl-quinoxalin-2(1H)-one (3-MeQ) were investigated in Ar-saturated solutions of Q and 3-MeQ over the concentration range of 0.08–1 mM and at various pH values in the range of 5–13 and containing also *tert*-butanol (0.5 M). Depending on the pH, pulse irradiation leads to different transient optical spectra.

3.1.1. Quinoxalin-2(1H)-one (Q): absorption spectra and kinetics at pH 7and 13.

Pulse radiolysis studies were performed with Ar-saturated solutions of Q (c~0.1 mM) containing also *tert*-butanol (0.5 M) at pH 7. Under these conditions, the main reactive species are hydrated electrons (e_{aq}^-). The transient absorption spectra recorded at pH = 7, at time intervals 120 ns, 1.6, 10, and 100 μs after the electron pulse are presented in Fig. 1. The transient absorption spectrum observed 120 ns after the electron pulse exhibits a broad band with a maximum located at $\lambda \approx 720$ nm, which can be unambiguously ascribed to the hydrated electron (e_{aq}^-)($\lambda_{max} = 720$ nm, $\varepsilon_{max} = 19{,}000$ M^{-1} cm^{-1})(Hug, 1981). This band disappeared completely within 2 μs and a new broad, almost flat band in the range 390–450 nm, with a very weakly pronounced maximum at $\lambda \approx 390$ nm appeared. The pseudo-first-order rate constant, determined from the time profile of the 720-nm decay, was found to be 4.4×10^6 s^{-1} (Fig. 1, inset in right bottom inset). The measured pseudo-first order rate constants show a linear dependence on the concentration of Q (Fig. 1; right bottom inset) with the slope representing the respective second-order rate constant for the reaction of e_{aq}^- with Q. The calculated second-order rate constant was found to be $k_{720} = (2.6 \pm 0.1) \times 10^{10}$ M^{-1} s^{-1} (Table 1). After disappearance of e_{aq}^-, the broad absorption band in the 390–450 nm range decayed uniformly in a first-order reaction with similar rate constants $k_{390} = 3.6 \times 10^5$ s^{-1} and $k_{460} = 3.3 \times 10^5$ s^{-1}, suggesting the presence of a single species responsible for this absorption band (Fig. 1, left inset). However, at this point in the exposition, we will not attempt

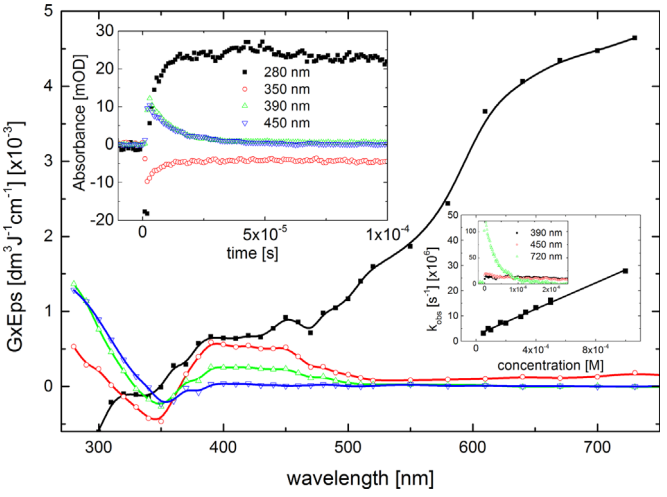

Fig. 1. Transient absorption spectra (uncorrected for the ground state absorption) recorded in Ar-saturated aqueous solution containing 0.1 mM Q and 0.5 M *tert*-butanol at pH 7 after 120 ns (■), 1.6 μs (◯), 10 μs (△), and 100 μs (▽) time delays after electron pulse. Insets: (left) Time profiles representing decays at $\lambda = 390$ nm (△) and $\lambda = 450$ nm (▽), formation at $\lambda = 280$ nm (■), and bleaching at $\lambda = 350$ nm (◯); (right) The plot of the observed pseudo-first-order rate constants of the decay of the 720-nm absorption (k_{obs}) as a function of Q concentration at pH 7. Inset of right inset: Time profiles representing time evolution of absorbances recorded at $\lambda = 390$, 450 and 720 nm at 0.1 mM concentration of Q.

Table 1
Rate constants for the reactions of hydrated electrons with Q and 3-MeQ and for the decay reactions of $Q^{\bullet -}$/3-$MeQ^{\bullet -}$ and $QH^{\bullet}$ and 3-$MeQH^{\bullet}$.

k	Q		3-MeQ	
	pH 7	pH 13	pH 7	pH 13
e^-_{aq} + Q/3-MeQ [$M^{-1}\,s^{-1}$]	$(2.6 \pm 0.1)^{a} \times 10^{10}$	$1.9 \pm 0.1^{b} \times 10^{10}$ $1.6 \pm 0.1^{a} \times 10^{10}$	$2.1 \pm 0.1^{a} \times 10^{10}$	$1.3 \pm 0.1^{b} \times 10^{10}$ $1.3 \pm 0.1^{a} \times 10^{10}$
$Q^{\bullet -}$/3-$MeQ^{\bullet -}$ and $QH^{\bullet}$/3-$MeQH^{\bullet}$ decay [s^{-1}]	3.6×10^{5}[c] 3.3×10^{5}[d] 3.0×10^{5}[e]	3.0×10^{5}[c] 3.2×10^{5}[d]	3.5×10^{5}[c] 3.5×10^{5}[d] 7.4×10^{5}[e]	3.0×10^{5}[c] 3.2×10^{5}[d]

[a] from the decay of absorption at $\lambda = 720$ nm.
[b] from the growth of the absorption at $\lambda = 390$ nm.
[c] from the decay of absorption at $\lambda = 390$ nm.
[d] from the decay of absorption at $\lambda = 450$ nm.
[e] from the growth of absorption at $\lambda = 280$ nm.

to assign the species responsible for the 390-nm absorption band. A bleaching signal was observed in the 320–370 nm range. Moreover, there was also an intense and broad absorption in the range 280–330 nm with no distinct λ_{max} up to 280 nm (Fig. 1) growing on the same time domain as the decay of the broad absorption band in the 390–450 nm range (Fig. 1, left top inset) with similar rate constant $k_{280} = 3.0 \times 10^5\ s^{-1}$. This might suggest a direct transformation of the 390-nm species into the 280-nm species.

The reaction of e^-_{aq} with Q was investigated at pH 13 in order to check to what extent the basic form of Q deprotonated at the nitrogen atom 1 (see Scheme 1) influences on e^-_{aq} reactivity and the spectral and kinetic characteristics of transients formed. The transient absorption spectra recorded at pH = 13, at time intervals 240 ns, 2, 24, and 240 μs after the electron pulse are presented in Fig. 2. A transient absorption spectrum recorded 240 ns after the pulse shows similar features to that observed at pH 7, and was assigned to e^-_{aq}. This band disappeared completely within 2 μs and a new broad band with a much better pronounced maximum at $\lambda_{max} = 390$ nm and higher intensity (in comparison to that at pH 7) appeared. The pseudo-first-order rate constant, determined from the time profile of the 720-nm decay, was found to be $2.4 \times 10^6\ s^{-1}$ (Fig. 2, inset in right bottom inset). The rate constant for the reaction of e^-_{aq} with Q, calculated from the linear plot presented in Fig. 2 (right bottom inset), was found to be $k_{720} = (1.6 \pm 0.1) \times 10^{10}\ M^{-1}\,s^{-1}$ (Table 1). Thus, the reactivity is less upon deprotonation. Since at pH 13, Q is present quantitatively as a monoanion (Scheme 1), the reason for this might be electrostatic repulsion between reagents and the increased electron density (decreased electron affinity) of the deprotonated molecule. As opposed to pH 7, the two kinetic traces, recorded at wavelengths 390 and 450 nm, are characterized by distinctly different time profiles (Fig. 2, inset in the right bottom inset). On one

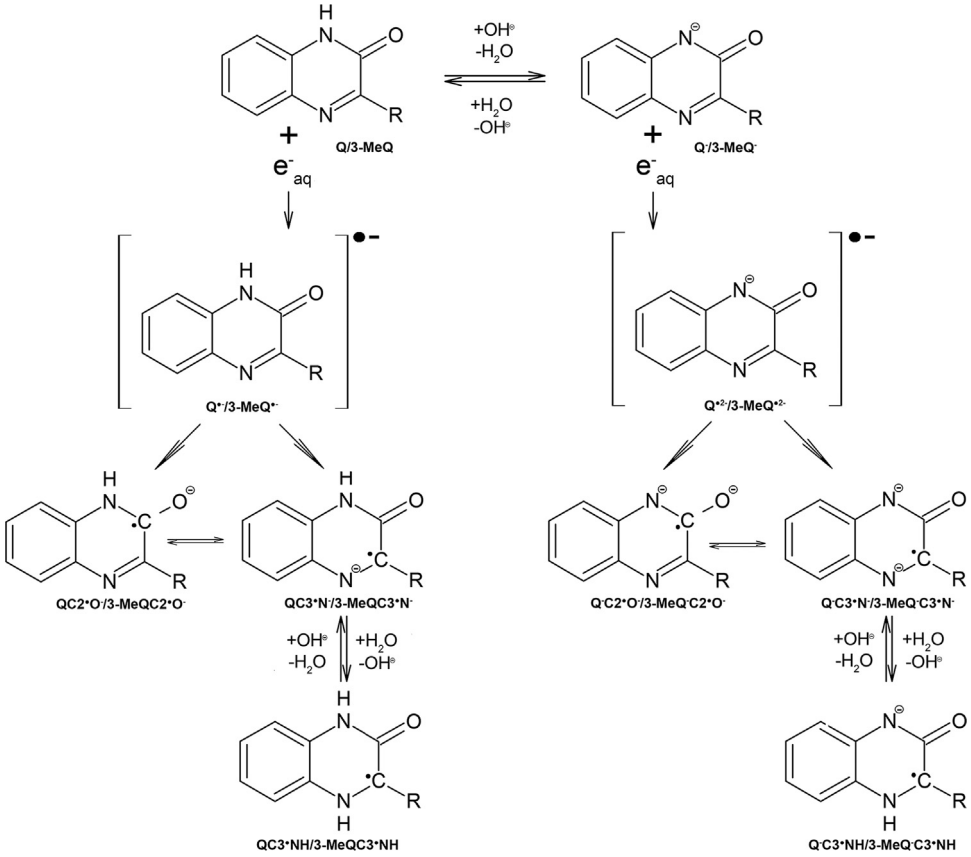

Scheme 1. Hydrated electron induced reduction of quinoxalin-2-one derivatives in aqueous solutions.

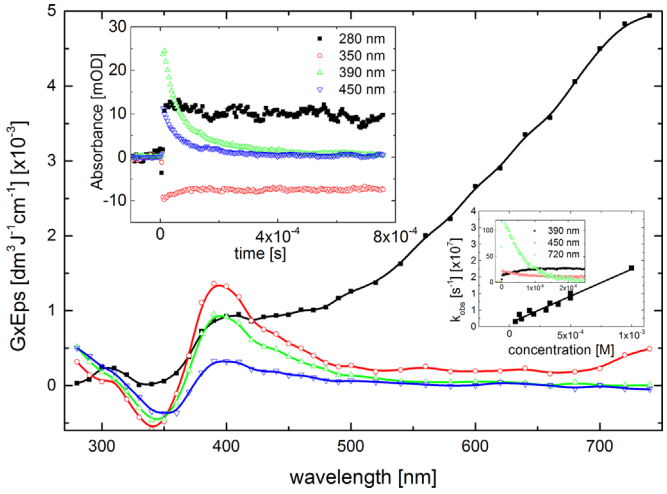

Fig. 2. Transient absorption spectra (uncorrected for the ground state absorption) recorded in Ar-saturated aqueous solution containing 0.1 mM Q and 0.5 M *tert*-butanol at pH 13 after 240 ns (■), 2 μs (◯), 20 μs (△), and 100 μs (▽) time delays after electron pulse. Insets: (left) Time profiles representing decays at λ=280 nm (■), 390 nm (△), and 450 nm (▽), and bleaching at λ=350 nm (◯); (right) The plot of the observed pseudo-first-order rate constants of the decay of the 720-nm absorption (k_{obs}) as a function of Q concentration at pH 13. Inset of right inset: Time profiles representing time evolution of absorbances recorded at λ=390, 450 and 720 nm at 0.1 mM concentration of Q.

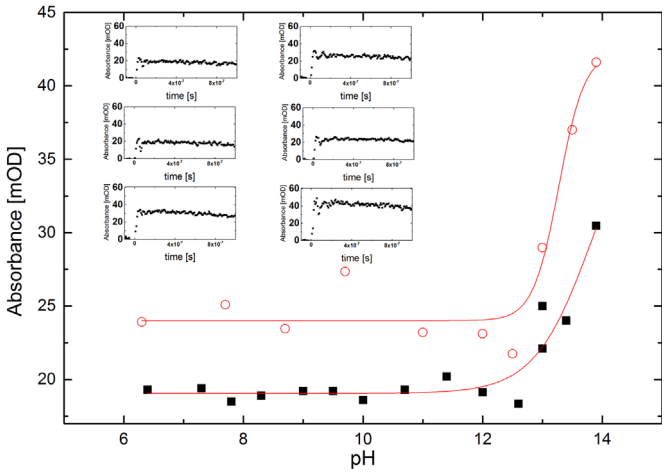

Fig. 3. Effect of pH on the absorbance at λ=390 nm measured by pulse radiolysis in Ar-saturated aqueous solution containing 1 mM Q (■) and 3-MeQ (◯) and 0.5 M *tert*-butanol at 0.5 μs after electron pulse. Insets: Time profiles representing time evolution of absorbances recorded at λ=390 nm for Q (left): pH 7.3 (top), 12 (middle), 13.9 (bottom) and 3-MeQ (right): pH 7.9 (top), 12 (middle), 13.9 (bottom).

hand, the kinetic trace at λ=390 nm grows and reaches a plateau within the same time domain as the kinetic trace at λ=720 nm showed a nearly complete decay. This behavior suggests that formation of the transient absorbing at λ=390 nm occurs at the expense of decay of the hydrated electrons. This band can be tentatively attributed to the electron adduct of Q (subsequently denoted by $Q^{\bullet -}$). To verify this assignment, the pseudo-first order rate constant were determined from the corrected time profiles of the 390-nm formation at various concentration of Q (Fig. 1S in Supporting information). This correction was necessary since it involves a contribution of the concomitant decay of hydrated electron which absorbs at this wavelength. The bimolecular rate constant calculated from the linear plot presented in the inset of Fig. 1S (in Supporting information) was found to be $k=(1.9\pm0.1)\times10^{10}$ M^{-1} s^{-1} (Table 1). This value is fairly close to that obtained from the 720-nm decays confirming former assignment. After disappearance of e^-_{aq}, the broad absorption band in the 390–450 nm range decayed uniformly in a first-order reaction with similar rate constants $k_{390}=3.0\times10^5$ s^{-1} and $k_{460}=3.2\times10^5$ s^{-1}, suggesting the presence of a single species responsible for this absorption band (Fig. 2, left top inset).

A bleaching signal is also observed in the 320–370 nm range. Moreover, there was also a broad absorption in the range 280–330 nm with no distinct λ_{max} up to 280 nm, however, with lower intensity (Fig. 2) in comparison to similar spectrum observed at pH 7 (Fig. 1). However, its formation is not correlated with a decay of the band with maximum at λ_{max}=390 nm as it was observed at pH=7 (Fig. 2, left top inset).

3.1.2. *Prototropic equilibrium of the radicals $Q^{\bullet -}$ and $QH^{\bullet}$*

Since the spectral and kinetic features of absorption bands recorded at pH 7 and 13 after completion of decay of hydrated electrons differ from each other, this behavior suggests the existence of the radical anion ($Q^{\bullet -}$) and its protonated conjugate $QH^{\bullet}$ in the prototropic equilibrium (5):

$$QH^{\bullet} \rightleftharpoons Q^{\bullet -} + H^+ \quad (5)$$

To determine the pK_a of the one-electron reduced products of Q, absorbance changes were followed at λ=390 nm where there is a most significant change with pH in the absorption spectrum of the transient. As shown in the left insets of Fig. 3, there is no change in the absorbance in the pH range where Q exists in two forms involved in the acid–base equilibrium with pK_a=9.08 (Chart 2), while above pH 13 the absorbance starts to increase up to pH 13.8.

Fig. 3 shows the representative sigmoidal curve for the change in absorbance on pH. The plateau was not reached, however, by fitting the curve to the appropriate function, the $pK_a \geq 13.5$ was obtained.

3.1.3. *3-methylquinoxalin-2(1H)-one (3-MeQ): absorption spectra and kinetics at pH 7 and 13*

The reaction of e^-_{aq} with 3-MeQ was investigated in order to check to what extent substitution at the carbon-3 by a methyl group in the pyrazine ring (see Chart 1) influences e^-_{aq} reactivity and the spectral and kinetics characteristics of the transients formed. The transient absorption spectra recorded in aqueous solutions containing 0.1 mM 3-MeQ at pH=7, at time intervals 120 ns, 1, 10, and 100 μs after the electron pulse are presented in Fig. 4. The transient absorption spectrum, obtained 120 ns after the electron pulse shows similar features to that observed at pH 7 with Q, and was assigned to e^-_{aq}. This band disappeared completely within 1 μs and a new broad band, almost flat in the range 390–450 nm, with a very weakly pronounced maximum at $\lambda\approx390$ nm appeared (Fig. 4), similarly to that observed for Q (Fig. 1). The pseudo-first-order rate constant, determined from the time profile of the 720-nm decay (k_{720}), was found to be 2.4×10^6 s^{-1} (Fig. 4, inset in the right inset). The rate constant for

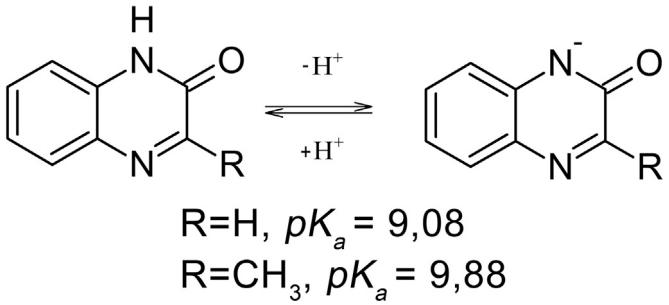

Chart 2. The acid–base equilibrium of quinoxalin-2-ones.

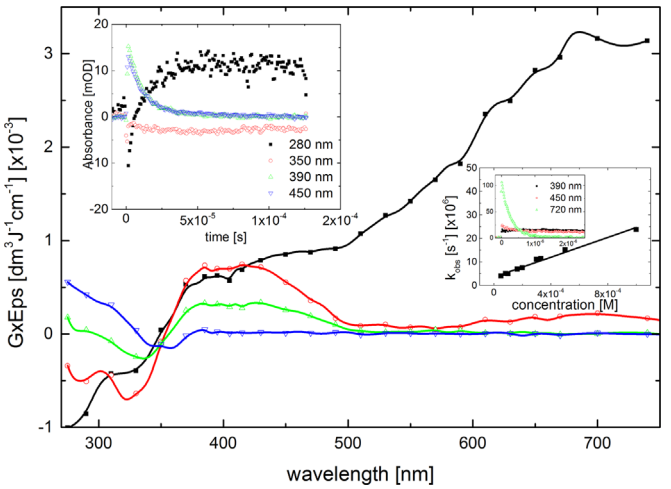

Fig. 4. Transient absorption spectra (uncorrected for the ground state absorption) recorded in Ar-saturated aqueous solution containing 0.1 mM 3-MeQ and 0.5 M *tert*-butanol at pH 7 after 120 ns (■), 1 μs (◯), 10 μs (△), and 100 μs (▽) time delays after electron pulse. Insets: (left) Time profiles representing decays at 390 nm (△) and 450 nm (▽), formation at $\lambda=280$ nm (■), and bleaching at $\lambda=330$ nm (◯); (right) The plot of the observed pseudo-first-order rate constants of the decay of the 720-nm absorption (k_{obs}) as a function of 3-MeQ concentration at pH 7. Inset of right inset: Time profiles representing time evolution of absorbances recorded at $\lambda=390$, 450 and 720 nm at 0.1 mM concentration of 3-MeQ.

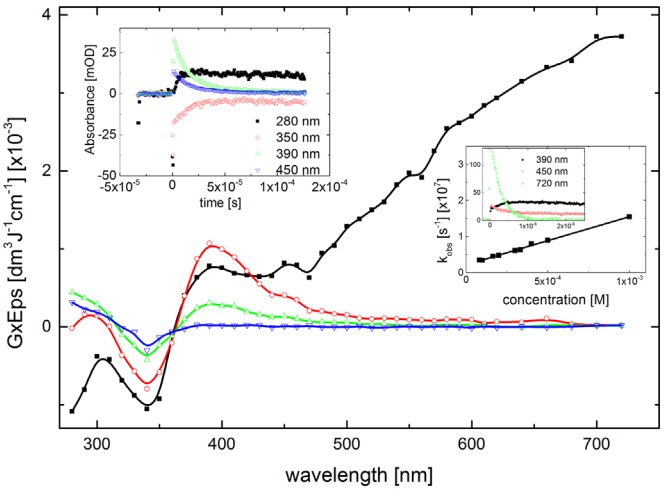

Fig. 5. Transient absorption spectra (uncorrected for the ground state absorption) recorded in Ar-saturated aqueous solution containing 0.1 mM 3-MeQ and 0.5 M *tert*-butanol at pH 13 after 120 ns (■), 2 μs (◯), 24 μs (△), and 240 μs (▽) time delays after electron pulse. Insets: (left) Time profiles representing decays at $\lambda=280$ nm (■), 390 nm (△), and 450 nm (▽), and bleaching at $\lambda=340$ nm (◯); (right) The plot of the observed pseudo-first-order rate constants of the decay of the 720-nm absorption (k_{obs}) as a function of 3-MeQ concentration at pH 13. Inset of right inset: Time profiles representing time evolution of absorbances recorded at $\lambda=390$, 450 and 720 nm at 0.1 mM concentration of 3-MeQ.

the reaction of e^-_{aq} with 3-MeQ, calculated from the linear plot presented in Fig. 4 (right inset), was found to be $k=(2.1\pm0.1)\times10^{10}$ M^{-1} s^{-1}. Contrary to Q where the time profile recorded at $\lambda=390$ nm did not reveal a concomitant growth of absorbance occurring on the same time domain, a weakly pronounced formation of absorbance at $\lambda=390$ nm was observed. (Fig. 4, inset in right inset). Similar correction taking into account contribution of the concomitant decay of hydrated electron does not emphasize the formation signal to the extent allowing the reliable fitting. After disappearance of e^-_{aq}, the broad absorption band in the 390–450 nm range decayed uniformly in a first-order reaction with similar rate constants $k_{390}=3.5\times10^5$ s^{-1} and $k_{460}=3.5\times10^5$ s^{-1}, suggesting the presence of a single species responsible for this absorption band (Fig. 4, left inset). A bleaching signal was observed in the 280–360 nm range. Moreover, there was also an intense and broad absorption in the range 280–330 nm with no distinct λ_{max} up to 280 nm (Fig. 4) growing on the same time domain as the decay of the broad absorption band in the 390–450 nm range (Fig. 4, left inset) with fairly similar rate constant $k_{280}=7.4\times10^5$ s^{-1}.

For the same reason, as for Q, the reaction of e^-_{aq} with 3-MeQ was investigated at pH 13. The transient absorption spectra recorded in aqueous solutions containing 0.1 mM 3-MeQ at pH=13, at time intervals 120 ns, 2, 24, and 240 μs after the electron pulse are presented in Fig. 5. A transient absorption spectrum recorded 240 ns after the pulse shows similar features to that observed at pH 7, and was assigned to e^-_{aq}. This band disappeared completely within 1 μs and a new broad band with a much better pronounced maximum at $\lambda_{max}=390$ nm (in comparison to that at pH 7) appeared. On the other hand, the spectral features are very similar to those observed for Q at the same pH (Fig. 2). The pseudo-first-order rate constant, determined from the time profile of the 720-nm decay, was found to be 3.5×10^6 s^{-1} (Fig. 5, inset in right inset). The rate constant for the reaction of e^-_{aq} with 3-MeQ, calculated from the linear plot presented in Fig. 5 (right bottom inset), was found to be $k=(1.3\pm0.1)\times10^{10}$ M^{-1} s^{-1}. Similarly as for Q, the pseudo-first order rate constants were also determined from the corrected time profiles of the 390-nm formation at various concentration of 3-MeQ (Fig. 2S in Supporting information). The bimolecular rate constant calculated from the linear plot presented in the inset of Fig. 2S (in Supporting information) was found to be $k=(1.3\pm0.1)\times10^{10}$ M^{-1} s^{-1}. This value is equal to that obtained from the 720-nm decays confirming former assignment of the 390-nm band to the respective radical anion (3-MeQ$^{\bullet-}$).

3.1.4. *Prototropic equilibrium of the radicals 3-MeQ$^{\bullet-}$ and 3-MeQH$^{\bullet}$*

Since the spectral and kinetic features of absorption bands recorded at pH 7 and 13 after completion of decay of hydrated electrons differ from each other (similarly to Q), this behavior suggests also the existence of the radical anion (3-MeQ$^{\bullet-}$) and its protonated conjugate 3-MeQH$^{\bullet}$ in the prototropic equilibrium (6):

$$\text{3-MeQH}^{\bullet} \rightleftharpoons \text{3-MeQ}^{\bullet-} + \text{H}^+ \quad (6)$$

To determine the pK_a of the one-electron reduced products of 3-MeQ, absorbance changes were also followed at $\lambda=390$ nm where there is a most significant change with pH in the absorption spectrum of the transient. As shown in the right insets of Fig. 3, there was no change in the absorbance in the pH range where 3-MeQ exists in two forms involved in the acid-base equilibrium with $pK_a=9.88$ (Chart 2) while above pH 13 the absorbance starts to increase up to pH 13.8. The plateau was not reached, however, by fitting the curve to the appropriate function, the $pK_a\geq13.5$ was obtained (Fig. 3).

3.2. *Radical anions and protonated radical anions: calculations*

In order to get the information about the most likely sites of the protonation in Q and 3-MeQ after electron addition, Mulliken charge densities (q_M) on heteroatoms O2 and N4 charge distribution in radical anions, spin densities in protonated radicals on nitrogen atom (N4), and enthalpies of the protonated radicals formation (ΔH_f) were calculated and listed in Tables S1 and S2 (in Supplementary material) and Table 2.). The data listed in Table S1 lead to the conclusion that the negative charge is efficiently distributed over O2 and N4 atoms with preferable location on O2 atoms in both compounds. However, the most favorable enthalpies of the protonated radical anions formation were found for the

Table 2
Enthalpies of the radical anions and hydrogenated radicals formation (ΔH_f) in Q and 3-MeQ.

Compound	Anion	N4H	OH	C3H	C5H	C6H	C7H	C8H
Q	−35.26	−0.57	5.42	2.58	9.41	10.02	10.53	8.41
3-MeQ	−43.50	−10.34	35.39	−1.31	0.54	0.86	1.68	−0.77

addition of protons at N4 for both compounds (Table 2).

With these information, a better insight can be obtained from relevant active electronic transitions and oscillator strengths for the respective radical anions and the respective protonated radicals at nitrogen (N4) and oxygen (O2) atoms. They are summarized in Table S3 (in Supplementary material). The compatibility between the experimentally observed and the calculated absorption spectra for the respective radical anions reproduce fairly well the main feature of the experimental spectra for $Q^{\bullet -}$ and 3-$MeQ^{\bullet -}$, i.e. the presence of the absorption maximum at 390 nm. On the other hand, the most intense calculated electronic transition for QN4H$^{\bullet}$ and 3-MeQN4H$^{\bullet}$ radicals are located <380 nm and <360 nm, i.e. in the region of the ground state absorption of both compounds. The lower signal of absorbance observed in this region is due to the higher bleaching signal caused by depletion of Q and 3-MeQ ground states. In order to overcome this obstacle, the experimental spectra were corrected for bleaching in the spectral range 280–380 nm. Both corrected spectra are characterized by strong absorption maxima located at $\lambda_{max}=350$ nm for both QN4H$^{\bullet}$ and 3-MeQN4H$^{\bullet}$ radicals (Fig. S3 in Supplementary material). These values are in a very good accordance with the location of the most intense calculated electronic transitions (Table S3 in Supplementary material).

4. Discussion

It is well established that hydrated electrons (e^-_{aq}) are highly reactive toward heterocyclic compounds (e.g. the purine and pyrimidine bases) due to presence of electron affinic nitrogen atoms and oxygen atoms in carbonyl groups (Buxton et al., 1988b). Therefore, it is not surprising that the rate constants for the reactions of e^-_{aq} with quinoxalin-2-ones (Q and 3-MeQ) were the diffusion controlled rates ($k>10^{10}$ M^{-1} s^{-1}) (Table 1). Several remarks can be made: firstly, the transient absorption spectra recorded at pH 7 after the decay of e^-_{aq} are similar for Q and 3-MeQ (Figs. 1 and 4). Secondly, the transient spectra recorded at pH 13 after the decay of e^-_{aq} are different from those recorded at pH 7, however, again similar for Q and 3-MeQ (Figs. 2 and 5). They have a distinct and much better pronounced maximum at $\lambda=390$ nm with substantially higher value of absorbance. Thirdly, for both compounds the absorbance recorded at $\lambda=390$ nm, after the decay of e^-_{aq}, is constant in the pH range 6.5–12.5 and then starts to grow rapidly (Fig. 3). Fourthly, at both pHs there are no spectral changes of any significance between 1 and 100 μs for Q and 3-MeQ.

Therefore, from the optical data one can conclude that the absorbing species present at pH 13 with $\lambda_{max}=390$ nm is mostly the electron adduct ($Q^{\bullet 2-}$/3-$MeQ^{\bullet 2-}$) (Scheme 1). This assignment is further confirmed by the similar bimolecular rate constant calculated from the growth of absorbance at $\lambda=390$ nm (Figs. S1 and S2 in Supplementary material) with those calculated from the decay of e^-_{aq} (Table 1). As a consequence, the absorption spectra observed at pH 7 have to be assigned to the products of protonation of the respective radical anions ($Q^{\bullet -}$/3-$MeQ^{\bullet -}$). The initial attack of e^-_{aq} is likely to occur at any of the electron-affinic heteroatoms (N4 atom and O atom in carbonyl group, both located in pyrazin-2-one ring) leading to the formation of the corresponding radical anions (QC2$^{\bullet}$O$^-$/3-MeQC2$^{\bullet}$O$^-$ and QC3$^{\bullet}$N$^-$/3-MeQC3$^{\bullet}$N$^-$) (Scheme 1). This is confirmed by the Mulliken charge distributions showing negative charge at O and N4 atoms (Table S1 in Supplementary material). These are the sites where protonation by water will probably occur preferentially since protonation is likely to occur first at a heteroatom but ultimate protonation may take place at carbon atoms (Hissung et al., 1981). Since quinoxalin-2-ones being (to some extent) structurally similar to purines and hypoxanthines, it can be reasonably assumed that radical anions derived from them are also rapidly protonated as in the case of adenine (Candeias and Steenken, 1992; Hissung et al., 1981; Visscher et al., 1987), guanine (Candeias et al., 1992; Nese et al., 1992), hypoxanthine (Aravindakumar et al., 1994), methyl derivative of xanthine (Rao et al., 1995), inosine (Aravindakumar et al., 1994), and 2′-deoxyinosine (Rao et al., 1996). This mechanism is apparently a general one for electron adducts of heterocyclic compounds (Candeias et al., 1992; Novais and Steenken, 1986). Thus, the rate of protonation of the radical anions in neutral solutions by H_2O may be at least as fast as the reaction of e^-_{aq} with quinoxalin-2-ones to yield the neutral heteroatom-protonated tautomers (QC2$^{\bullet}$OH/3-Me QC2$^{\bullet}$OH and QC3$^{\bullet}$NH/3-Me QC2$^{\bullet}$NH) (Scheme 1). Due to much higher negative charge at O atom in comparison to N4 atom, one might expect that formation of QC2$^{\bullet}$OH/3-MeQC2$^{\bullet}$OH tautomers over QC3$^{\bullet}$NH/3-Me QC2$^{\bullet}$NH tautomers will be preferential (Table S1 in Supporting material). Interestingly, the calculated enthalpies show that formation of the former tautomers is thermodynamically unfavorable (Table 2). This fact, however, does not speak against the primary formation of the QC2$^{\bullet}$O$^-$/3-MeQC2$^{\bullet}$O$^-$ radical anions. Fast mesomerization to QC3$^{\bullet}$N$^-$/3-MeQC3$^{\bullet}$N$^-$ radical anions can be considered as an alternative transformation pathway (Scheme 1).

Moreover, it is well known that the site of protonation strongly affects the pK_a values of the protonated radical anions derived from nucleobases (Steenken, 1992). The pK_a values of the O-protonated radical anions of uracil and thymine are near 7 (Deeble et al., 1985) (Shragge and Hunt, 1974). On the other hand, with radical anions of cytosine (Hissung, von Sonntag 1979) and guanosine (Candeias et al., 1992), rapid protonation by water occurs at nitrogen atoms and the pK_a values of their N-protonated radicals are higher than 13 (Naumov and von Sonntag, 2008).

From the representative sigmoidal curves for the change of absorbances on pH at $\lambda=390$ nm, the pK_a of the phototropic equilibrium involving protonated radical anions (QH$^{\bullet}$/3-MeQH$^{\bullet}$) and radical anions ($Q^{\bullet -}$/3-$MeQ^{\bullet -}$) was found to be located at pH > 13 (Fig. 3). Based on these observations taken together with previous considerations, one can conclude that protonated radical anions at nitrogen atom (N4) are the most stable hydrogenated radicals in both quinoxalin-2-one molecules. In 3-MeQ, these radicals are additionally stabilized by the synergestic effect of the carbonyl group (electron withdrawing) and the methyl group (electron-donating) known as the captodative effect (Viehe et al., 1985).

Additional support for the predominant presence of the protonated radical anions at nitrogen atom N4 with the radical site located at carbon atom C3 came from the analysis of photochemically generated stable products in acetonitrile solutions containing 3-MeQ derivatives and phenylglycine ($PhNHCH_2COOH$). The stable product resulting from the recombination of the former radical with the phenyl-aminoalkyl radical ($PhNHCH_2^{\bullet}$) was unambiguously identified (De la Fuente et al., 2013). What is more, protonation of the nitrogen atom N4 was postulated during a pH dependent two-electron reduction process of quinoxalin-2-ones (Zimpl et al., 2012).

Careful analysis of charge distributions in $Q^{\bullet -}$/3-$MeQ^{\bullet -}$ reveals

that the negative charge is also located on the carbon atoms (Table S1 in Supplementary material) and thus allowing their protonation. However, the calculated enthalpies show that their formation are also thermodynamically disfavored (except C3 and C8 in 3-MeQ$^{\bullet-}$).

Acknowledgments

Financial support under Polish National Science Centre (NCN) Grant PRELUDIUM no. 2014/15/N/ST4/02914 and FONDECYT Grant no. 1150567 is greatly acknowledged.

Appendix A. Supplementary material

Supplementary data associated with this article can be found in the online version at http://dx.doi.org/10.1016/j.radphyschem.2015.12.008.

References

Ajani, O.O., Obafemi, C.A., Nwinyi, O.C., Akinpelu, D.A., 2010. Microwave assisted synthesis and antimicrobial activity of 2-quinoxalinone-3-hydrazone derivatives. Bioorganic Med. Chem. 18, 214–221.
Aravindakumar, C.T., Mohan, H., Mudaliar, M., Rao, B.S.M., Mittal, J.A., Schuchmann, M.N., Von Sonntag, C., 1994. Addition of e^-_{aq} and H atoms to hypoxanthine and inosine and the reactions of a-hydroxyalkyl radicals with purines. A pulse radiolysis and product analysis study. Int. J. Radiat. Biol. 66, 351–365.
Bobrowski, K., 2005. Free radicals in chemistry, biology and medicine: contribution of radiation chemistry. Nukleonika 50 (Suppl 3), S67–S76.
Buxton, G.V., 2008. An overview of the radiation chemistry of liquids. In: Spotheim-Maurizot, M., et al. (Eds.), Radiation Chemistry: From Basics to Applications in Material and Life Sciences. EDP Sciences, pp. 3–16.
Buxton, G.V., Greenstock, C.L., Helman, W.P., Ross, A.B., 1988a. Critical review of rate constants for reactions of hydrated electrons, hydrogen atoms and hydroxyl radicals ($^{\bullet}OH/O^{\bullet-}$) in aqueous solution. J. Phys. Chem. Ref. Data 17, 513–886.
Buxton, G.V., Mulazzani, Q.G., Ross, A.B., 1988b. Critical review of rate constants for reactions of transients from metal ions and metal complexes in aqueous solutions. J. Phys. Chem. Ref. Data 24, 1035–1349.
Candeias, L.P., Steenken, S., 1992. Electron adducts of adenine nucleosides and nucleotides in aqueous solution: Protonation at two carbon sites (C2 and C8) and intra- and intermolecular catalysis by phosphate. J. Phys. Chem. 96, 937–944.
Candeias, L.P., Wolf, P., O'Neill, P., Steenken, S., 1992. Reaction of hydrated electrons with guanine nucleosides: fast protonation on carbon of the electron adduct. J. Phys. Chem. 96, 10302–10307.
Carta, A., Piras, S., Loriga, M., Paglietti, G., 2006. Chemistry, biological properties and SAR analysis of quinoxalinones. Mini-Rev. Med. Chem. 6, 1179–1200.
Carta, A., Sanna, P., Loriga, M., Setzu, M.G., La Colla, P., Loddo, R., 2002. Synthesis and evaluation for biological activity of 3-alkyl and 3-halogenoalkyl-quinoxalin-2-ones variously substituted. Part 4. Il Farmaco 57, 19–25.
De la Fuente, J.R., Cañete, A., Jullian, C., Saitz, C., Aliaga, C., 2013. Unexpected imidazoquinoxalinone annulation products in the photoinitiated reaction of substituted-3-methyl-quinoxalin-2-ones with N-phenylglycine. Photochem. Photobiol. 89, 1335–1345.
De la Fuente, J.R., Cañete, A., Saitz, C., Jullian, C., 2002. Photoreduction of 3-phenylquinoxalin-2-ones by amines. Transient-absorption and semiempirical quantum-chemical studies. J. Phys. Chem. A 106, 7113–7120.
De la Fuente, J.R., Cañete, A., Zanocco, A.L., Saitz, C., Jullian, C., 2000. Formal hydride transfer mechanism for photoreduction of 3-phenylquinoxalin-2-ones by amines. Association of 3-phenylquinoxalin-2-one with aliphatic amines. J. Org. Chem. 65, 7949–7958.
Deeble, D.J., Das, S., Von Sonntag, C., 1985. Uracil derivatives: sites and kinetics of protonation of the radical anions and the UV spectra of the C(5) and C(6) H-atom adducts. J. Phys. Chem. 89, 5784–5788.
El-Sabbagh, O.L., El-Sadek, M.E., Lashine, S.M., Yassin, S.H., El-Nabtity, S.M., 2009. Synthesis of new 2(1H)-quinoxalinone derivatives for antimicrobial and anti-inflammatory evaluation. Med. Chem. Res. 18, 782–797.
Hirai, H., Takahashi-Suziki, I., Shimomura, T., Fukusawa, K., Machida, T., Takaki, T., Kobayashi, M., Eguchi, T., Oki, H., Arai, T., Ichikawa, K., Hasako, S., Kodera, T., Kawanishi, N., Nakatsuru, Y., Kotani, H., Iwasawa, Y., 2011. Potent anti-tumor activity of a macrocycle-quinoxalinone class pan-Cdk inhibitor in vitro and in vivo. Investig. New Drugs 29, 534–543.
Hissung, A., von Sonntag, C., 1979. The reaction of solvated electron with cytosine, 5-methylcytosine and 2′-deoxycytidine in aqueous solution. The reaction of the electron adduct intermediates with water, p-nitroacetophenone and oxygen. A pulse spectroscopic and pulse conductometric study. Int. J. Radiat. Biol. 35, 449–458.
Hissung, A., von Sonntag, C., Veltwisch, D., Asmus, K.-D., 1981. The reactions of the 2′-deoxyadenosine electron adduct in aqueous solution. The effects of the radiosensitizer p-nitroacetophenone. A pulse spectroscopic and pulse coonductometric study. Int. J. Radiat. Biol. 39, 63–71.
Hug, G.L., 1981. Optical Spectra of Nonmetallic Inorganic Transient Species in Aqueous Solutions. National Institute of Standards and Technology, Gaithersburg, MD.
Ingale, S.J., Gupta, S., Upmanyu, N., Pande, M., 2007. Synthesis and biological evaluation of some 4-substituted quinoxalinones. Asian J. Chem. 19, 3797–3802.
Koth, E.R., Anwar, M.A., Soliman, M.S., Salama, M.A., 2007. Synthesis and reactions of some novel quinoxalines for anticancel evaluation. Phosphorous Sulfur Silicon Relat. Elem. 182, 1119–1130.
Kucybala, Z., Paczkowski, J., 1999. 3-Benzoyl-7-diethylamino-5-methyl-1-phenyl-1H-quinoxalin-2-one: an effective dyeing photoinitiator for free radical polymerization. J. Photochem. Photobiol. A: Chem. 128, 135–138.
Kucybala, Z., Pyszka, I., Paczkowski, J., 2000. Development of new dyeing photoinitiators for free radical polymerization based on the 1H-pyrazolo[3,4-b]quinoxaline skeleton. J. Chem. Soc. Perkin Trans. 2, 1559–1567.
Lawrence, D.S., Copper, J.E., Smith, C.D., 2001. Structure-activity studies of substituted quinoxalinones as multiple-drug-resistance antagonists. J. Med. Chem. 44, 594–601.
Meyer, E., Joussef, A.C., de Souza, L.D.P., 2006. Synthesis of new 1,2,4- and 1,3,4-oxadiazole derivatives as potential nonpeptide angiotensin II receptor antagonists. Synth. Commun. 36, 729–741.
Mori, Y., Hirokawa, T., Aoki, K., Satomi, H., Takeda, S., Aburada, M., Miyamoto, K., 2008. Structure activity relationships of quinoxalin-2-one derivatives as platelet-derived growth factor-β receptor (PDGFβ R) inhibitors, derived from molecular modeling. Chem. Pharm. Bull. 56, 682–687.
Naumov, S., von Sonntag, C., 2008. The energetics of rearrangement and water elimination reactions in the radiolysis of the DNA bases in aqueous solution (e^-_{aq}, and $^{\bullet}OH$ attack): DFT calculations. Radiat. Res. 169, 353–363.
Nese, C., Yuan, P., Schuchmann, H.-P., von Sonntag, C., 1992. Electron transfer from nucleobase electron adducts to 5-bromouracil. Is guanine a ultimate sink for the electron in irradiated DNA. Int. J. Radiat. Biol. 62, 527–541.
Nishio, T., 1990. Photochemical reactions of quinoxalin-2-ones and related compounds. J. Chem. Soc. Perkin Trans. 1, 565–570.
Novais, H.M., Steenken, S., 1986. ESR studies of electron and hydrogen adducts of thymine and uracil and their derivatives and of 4,6-dihydropyrimidines in aqueous solution. Comparison with data from solid state. The protonation at carbon of the electron adducts. J. Am. Chem. Soc. 108, 1–6.
Rao, R.R., Aravindakumar, C.T., Rao, B.S.M., 1995. Transformation reactions of the electron adducts of methyl derivatives of xanthine in aqueous solutions by pulse radiolysis. J. Chem. Soc. Faraday Trans. 91, 615–621.
Rao, R.R., Aravindakumar, C.T., Rao, B.S.M., Mohan, H., Mittal, J.A., 1996. Kinetics and spectral properties of electron adducts of 2′-deoxyinosine: a comparison with other purine nucleosides. J. Chem. Soc. Perkin Trans. 2, 1077–1080.
Ries, U.J., Priepke, H.W.M., Hauel, N.H., Handschuh, S., Mihm, G., Stassen, J.M., Wienen, W., Nar, H., 2003. Heterocyclic thrombin inhibitors. Part 2: quinoxalinone derivatives as novel, potent antithrombotic agents. Bioorganic Med. Chem. Lett. 13, 2297–2302.
Sanna, P., Carta, A., Loriga, M., Zanetti, S., Sechi, L., 1998. Synthesis of substituted 2-ethoxycarbonyl- and 2-carboxyquinoxalin-3-ones for evaluation of antimicrobial and anticancer activity. Il Farmaco 53, 455–461.
Sanna, P., Carta, A., Loriga, M., Zanetti, S., Sechi, L., 1999. Preparation and biological evaluation of 6/7-trifluoromethyl(nitro)-, 6,7-difluoro-3-alkyl (aryl)-substituted-quinoxalin-2-ones. Part 3. Il Farmaco 54, 169–177.
Schuler, R.H., Patterson, L.K., Janata, E., 1980. Yield for the scavenging of hydroxyl radicals in the radiolysis of nitrous oxide-saturated aqueous solutions. J. Phys. Chem. 84, 2088–2090.
Shragge, P.C., Hunt, J.W., 1974. A pulse radiolysis study of the free radical intermediates in the radiolysis of uracil. Radiat. Res. 60, 233–249.
Skotnicki, K., De la Fuente, J.R., Cañete, A., Bobrowski, K., 2014. Spectral and kinetic properties of radicals derived from oxidation of quinoxalin-2-ones and its methyl derivative. Molecules 19, 19152–19171.
Steenken, S., 1992. Electron-transfer-induced acidity/basicity and reactivity changes of purine and pyrimidine bases, consequences of redox processes for DNA base pairs. Free Radic. Res. Commun. 16, 349–379.
Ulrich, R.G., Bacon, J.A., Cramer, C.T., Petrella, D.K., Sun, E.L., Meglasson, M.D., Holmuhamedov, E., 1998. Disruption of mitochondrial activities in rabbit and human hepatocytes by a quinoxalinone anxiolytic and its carboxylic acid metabolite. Toxicology 131, 33–47.
Viehe, G., Janousek, Z., Merenyi, R., Stella, L., 1985. The captodative effect. Acc. Chem. Res. 18, 148–154.
Visscher, K.J., De Haas, M.P., Loman, H., Vojnovic, B., Warman, J.M., 1987. Fast protonation of adenosine and of its radical anion formed by hydrated electron attack; a nanosecond optical and dc-conductivity pulse radiolysis study. Int. J. Radiat. Biol. 52, 745–753.
Willardsen, J.A., Dudley, D.A., Cody, W.L., Chi, L.G., McClanahan, T.B., Mertz, T.E., Potoczak, R.E., Narasimhan, L.S., Holland, D.R., Rapandalo, S.T., Edmunds, J.J., 2004. Design, synthesis, and biological activity of potent, and selective inhibitors of blood coagulation factor Xa. J. Med. Chem. 47, 4089–4099.
Xu, B., Sun, Y., Guo, Y., Cao, Y., Yu, T., 2009. Synthesis and biological evaluation of N4-(hetero)arylsulfonylquinoxalinones as HIV-1 reverse transcriptase inhibitors. Med. Chem. 17, 2767–2774.
Zimpl, M., Skopalova, J., Jirovsky, D., Bartak, P., Navratil, T., Sedonikova, J., Kotoucek, M., 2012. Electrochemical behavior of quinoxalin-2-one derivatives at mercury electrodes and its analytical use. Sci. World J., 409378.